High spatial resolution CO_2 measurement using low-cost commercial sensors in Seoul megacity

JaeYoung Park[1], Jinho Ahn[1*], Jeongeun Kim[1], Nasrin Salehnia[1]

[1]School of Earth and Environment Sciences, Seoul National University, Seoul, 08826, Republic of Korea

Correspondence to: Jinho Ahn (jinhoahn@snu.ac.kr)

Abstract. Carbon dioxide (CO_2) is the most significant anthropogenic greenhouse gas. However, tracking CO_2 levels can be challenging due to the uneven distribution of concentrations and the high cost of sensors. In this study, we explored several correction techniques to enable the large-scale use of affordable CO_2 sensors, thereby enhancing the spatial resolution. We found that the low-cost CO_2 sensor (HT-2000) closely aligned with the trends observed in data from a more accurate sensor (LI-840a). By applying multiple-point linear regression, we reduced the root mean square error (RMSE) to only 1–2% of the measured value, which is accurate enough for urban monitoring at a local scale. Using a large network of low-cost sensors, we were able to map CO_2 concentration in detail, capture fine spatial variations, and gain a clearer understanding of emission patterns at an urban road intersection and within a tunnel.

1 Introduction

Carbon dioxide (CO_2) is the most significant anthropogenic greenhouse gas and the primary driver of the global climate crisis (IPCC, 2021). Currently, a larger proportion of the global population resides in urban areas than in rural regions. Urbanisation leads to disproportionate resource consumption in cities, contributing to approximately 70% of global CO_2 emissions linked to energy use (Rosenzweig et al., 2010; Gurney et al., 2020). Seoul is a megacity, home to approximately 20% of the country's population despite occupying only 0.6% of the total land area (Seoul Metropolitan Government, 2023; Korean Ministry of Culture, Sports and Tourism, 2024). Seoul directly emitted 18,565 ktonCO_2 in 2022; The two most important direct sources of CO_2 for it are buildings (commercial/residential) and road traffic; those are responsible for nearly 80% of all CO_2 emissions within Seoul. In addition to that, Seoul was indirectly responsible for 19,727 ktonCO_2 in 2022, where about 82% of which is from power generation (Seoul Carbon Neutrality Support Center, 2022). Monitoring urban CO_2 emissions is a critical step toward implementing effective reduction strategies and mitigating global warming; for example, accurate high-resolution monitoring of urban CO_2 may reveal new point sources within the urban landscape, usually treated as a single plane source. As well, it may reveal important phenomena that influences local CO_2 level. However, the highly diverse and heterogeneous land-use patterns in urban areas (Band et al., 2005; Olivo et al., 2017), combined with significant temporal variability in energy consumption (Olivo et al., 2017), result in substantial spatial and temporal variations in surface CO_2 concentrations (Park et al., 2022; Hong et al, 2023). This variability complicates accurate estimation of CO_2 fluxes at small scales using a top-down

approach, which begins with concentration of CO_2 and calculates flux from it, making urban flux calculations predominantly reliant on a bottom-up methods, which relies on statistic data to compile CO_2 inventories.

Previous studies have indicated that bottom-up emission estimates often suffer from considerable uncertainties. A comparison between downscaled global inventories frequently reveals differences exceeding 100% at the urban scale (Gately and Hutyra, 2017), and model results show substantial discrepancies when compared with bottom-up inventories (Gurney et al., 2019). Numerous attempts have been made to measure urban CO_2 concentrations. One approach is satellite monitoring, which provides an accurate snapshot of CO_2 concentration at kilometre-scale spatial resolution (Kiel et al., 2021; Kort et al., 2012). However, a major limitation of satellites is poor temporal resolution. All currently active greenhouse gas-monitoring satellites operate in low-Earth orbit, making continuous regional monitoring impossible. This limitation hinders the identification of diurnal patterns and obscures precise CO_2 sources. Furthermore, satellites measure total column CO_2, whose vertical profile varies significantly in the lower atmosphere (Roche et al., 2021), introducing additional inaccuracy. To achieve continuous temporal measurements, it is necessary to deploy gas-monitoring stations within cities (Imasu et al., 2018) or utilise mobile platforms. Stationary monitoring stations offer superior temporal resolution and are useful for capturing daily, monthly, or seasonal patterns. However, budgetary constraints often limit spatial resolution, leading prior research efforts to rely on medium-precision, medium-cost sensors (Spinelle et al., 2017; Arzoumanian et al., 2019).

This study presents an approach using a very low-cost, pre-assembled CO_2 monitoring kit (85 USD; including nondispersive infrared (NDIR) CO_2 sensor, relative humidity sensor, and temperature sensor) to enable high-resolution CO_2 measurements in urban environments. We also present 2D spatial movies of ambient CO_2 levels measured in urban Seoul and within a tunnel in the city, and visualizations made using the resulting data. Time-series data were corrected post hoc using a high-precision NDIR sensor (LI-840a), and we discuss methodologies for implementing effective correction schemes.

2 Materials and methods

2.1 Instrument description

The HT-2000 is a commercially available device manufactured by Dongguan Xintai Instrument Co. Its primary component is a SenseAir S8 CO_2 sensor, which operates on the principle of the NDIR absorption. This sensor quantifies CO_2 concentrations by measuring infrared absorbance, following the Beer–Lambert law. The sensor has a measurement range of 400–2000 ppm, with an extended range of up to 10,000 ppm, albeit with reduced accuracy at higher concentrations (SenseAir, 2025). According to the manufacturer, its accuracy is within ±70 ppm or ±3% of the reading. With its relatively low-cost (85 USD; HTi, 2023) compared to the high-accuracy sensors commonly used for similar applications (usually > 1000s USD), the HT-2000 provides a cost-effective solution for broad laboratory deployment when suitable correction methods are applied to improve its accuracy. Because the HT-2000 sensors can store only 12,700 data points and the battery supports roughly 48 h of continuous operation, the measurement period is necessarily limited. However, much longer measurements would be possible if the sensors could be supplied with continuous power.

In contrast, the LI-840a CO_2 analyser is a high-performance NDIR CO_2/H_2O sensor manufactured by LI-COR Environmental a wide variety of applications. Unlike the HT-2000, which is an open-path sensor, the LI-840a operates as a closed-path system using a custom-made optical bench. However, both sensors are based on the same fundamental NDIR principles. According to the manufacturer, LI-840a has an accuracy better than 1.5% of the reading value and RMS noise level below 1 ppm. In addition, from our experience, the sensor's precision can be improved to significantly surpass the manufacturer's specifications, often yielding fluctuations of approximately 0.1 ppm. Despite its superior performance, the high cost (> 3000 USD) of the LI-840a unit limits the number of units that can be deployed simultaneously.

2.2 Site description and measurement procedure

We selected two locations within Seoul (Bongcheon Intersection and Guryong Tunnel) for our measurements. We prioritized areas likely to show strong spatial and temporal variability in CO_2, such as high-traffic zones and districts with a high density of commercial buildings.

The Bongcheon Intersection is located directly above the Seoul National University subway station, which serves approximately 40,000 passengers daily (Figure S1). Twenty locations in the vicinity of the station were selected for sensor placement, representing the area's diverse land-use patterns. Among these, four points were located directly on the junction, and two at nearby traffic crossings. Additionally, six points were situated near or on residential buildings, while the remaining eight were near or on commercial buildings (Figure 1).

CO_2 levels around the Bongcheon Intersection were measured on 8 June 2022 and 8 February 2023 using 20 HT-2000 meters. A pre-calibrated LI-840a analyser served as the reference instrument for correcting the HT-2000 sensor data. The LI-840a was calibrated using a two-point method with two different mixed gas canisters with known CO_2 concentrations (398 and 990 ppm). We then corrected the 20 HT-2000 meters with multiple-point linear regression; the data for regression was obtained by placing all HT-2000 sensors and the LI-840a sensor at the same place, near the centre of the intersection (Figure S2).

Air was pumped through the LI-840a at a flow rate of 3 L/min using a $MgClO_4$ water vapour trap and aluminium tubing with a polymer coating, whereas the HT-2000 meters were exposed to open air. A 137-second moving average was applied to the LI-840a data for calculating the instrument specific time delay for individual HT-2000 meter, ranging from 7 to 43 s. We have tried various lengths of smoothing window using a FOR loop for both correction periods and found out that 137 seconds yielded the least RMSE difference between the LI-COR and HT-2000 instruments. The time delay for each HT-200 was also calculated algorithmically, by finding the "best match" between the LI-COR and HT-2000. The smoothed LI-840a data were used to calibrate the vapour-corrected data from the HT-2000 meters (vapour pressure was removed using temperature, relative humidity, and average atmospheric pressure recorded by the HT-2000, as well as Tetens' approximation equation for saturation vapour pressure). This correction was performed using multiple-point linear regression. Finally, the HT-2000 meters were distributed and deployed at the Bongcheon Intersection for 1 h to collect data and create a detailed CO_2 concentration map (Figure S1).

Figure 1: Map of Bongcheon Intersection. Marked are correction data spots (red triangle [2022] and square [2023]) and HT-2000 measurement spots (blue circles for both dates). One measurement spot (out of 20) is not depicted due to the sensor placed in the spot having problems in both 2022 and 2023 measurements. © OpenStreetMap Contributors 2024. Distributed under the Open Data Commons Open Database License (ODbL) v1.0.

The Guryong Tunnel is a pair of one-way tunnels located between the Gangnam and Seocho districts in Seoul. It experiences heavy traffic, with over 40 vehicles passing in a single direction each minute. CO_2 levels in the Guryong Tunnel were measured on 25 July 2024 and 21 November 2024, using 22 HT-2000 devices on 25 July and 21 devices on 21 November. To correct the results, all HT-2000 devices were placed in a sealed box the day before the measurements. The box was then flushed with air containing known CO_2 concentrations (990 and 398 ppm) for 1 h to perform a two-point correction for each meter. The devices were powered overnight.

In addition, for the November 2024 experiments only, an LI-840a device was used to correct the HT-2000 devices using the multi-point linear regression method, following the same procedure as at the Bongcheon Intersection. Dat for correction were obtained at the tunnel exit for 1 h between 09:30 and 10:30 AM. Then, HT-2000 meters were placed inside the tunnel (Seoul-bound direction) at semi-regular intervals, where CO_2 concentration were recorded for 1.5 h on 25 July (9:30 AM – 11:00 AM) and 20 h on 21 November (11:00 AM – 22 November 7:00 AM).

The November data were corrected using two different methods: two-point interpolation and multi-point linear regressions. The results of these two methods were compared to assess their efficacy. The July measurement data were corrected using only a two-point method. Atmospheric pressure was not considered relevant because of its short measurement duration. Similarly, humidity and temperature were excluded from the analysis because of high uncertainty in these measurements, and the potential improvement from including these factors was minimal compared with the associated errors (see section 2.3.3).

Figure 2. Aerial photograph of Guryong tunnel and the location of placed HT-2000 sensors. Map data © Airbus 2025. The tick marks indicate the location of the sensors placed; 0 indicates the entrance to the tunnel.

2.3 Data correction method

We used two correction methods for the HT-2000 data. At Bongcheon Intersection (2022 Jun 08 and 2023 Feb 08), only the multi-point linear regression method was applied. For the initial Guryong Tunnel measurement on 2025 Jul 25, a two-point linear regression was adopted for a simpler correction. In contrast, the 2024 Nov 21 Guryong Tunnel dataset was processed using both methods to compare their performance.

2.3.1 Multi-point linear regression

Linear regression is a statistical technique to estimate the relationship between the dependent variable (the CO_2 concentration measured by LI-840a) and one or more independent variables (CO_2 concentration, temperature, and humidity measured by a (single) HT-2000 sensor). The model takes the following form:

$$y_i = \beta_0 + \beta_1 x_{i1} + \cdots + \beta_p x_{ip} + \varepsilon_i$$

where y represents the response variable, x represents the predictors, β denotes the regression coefficients, and ε is the error term. The subscript i refers to the time point in the time-series regression. In this experiment, y_i corresponds to the CO_2 concentration measured at time i using the LI-840a analyser, while, x_{i1}, x_{i2}, and x_{i3} represent the CO_2 concentration, temperature, and humidity (measured by each HT-2000), respectively. The model can be expressed in matrix form as follows:

$$\mathbf{y} = \mathbf{X}\boldsymbol{\beta} + \boldsymbol{\varepsilon}$$

where,

$$\mathbf{y} = \begin{bmatrix} y_1 \\ y_2 \\ \vdots \\ y_n \end{bmatrix}, \mathbf{X} = \begin{bmatrix} 1 & x_{11} & \cdots & x_{1p} \\ 1 & x_{12} & \cdots & x_{2p} \\ \vdots & \vdots & \ddots & \vdots \\ 1 & x_{n1} & \cdots & x_{np} \end{bmatrix}, \boldsymbol{\beta} = \begin{bmatrix} \beta_0 \\ \beta_1 \\ \beta_2 \\ \vdots \\ \beta_p \end{bmatrix}, \boldsymbol{\varepsilon} = \begin{bmatrix} \varepsilon_1 \\ \varepsilon_2 \\ \vdots \\ \varepsilon_n \end{bmatrix}$$

2.3.2 Two-point correction

The two-point correction method is an approximation method that utilises two known reference points (high and low) and assumes that the sensor response is linear within this range. It was used to correct HT-2000 sensors post-measurement. The equation is as follows:

$$\mathrm{x_{sample}} = \mathrm{x_{std1}} + \frac{\mathrm{x_{std1}} - \mathrm{x_{std2}}}{\mathrm{y_{std1}} - \mathrm{y_{std2}}} \left(\mathrm{y_{sample}} - \mathrm{y_{std1}}\right)$$

where x denotes the actual value (or the assigned value for standard air); y represents the value displayed by the sensor; x_{std1} and x_{std2} are the known reference values for the high and low points, respectively; y_{std1} and y_{std2} are the corresponding sensor readings for the high and low points, respectively; and y_{sample} is the sensor reading for the corrected sample.

2.3.3 Comparison of correction methods

To evaluate whether the multi-point linear regression method produces better results, we compared it with a flat-shift method. For the Bongcheon Intersection measurements, the measurement error was assumed to be constant. In the flat-shift method, each HT-2000 device was treated as having a fixed bias relative to the actual CO_2 concentration, and this bias was used for the correction. During correction, the data from individual HT-2000 unit were averaged and compared with the average of LI-840a data. The HT-2000 data were then adjusted to match this average. For comparison, a multi-point linear regression method was also used to correct the HT-2000 devices. Both methods significantly reduced the RMSE values, with the multi-point linear regression method reducing the median RMSE by about 0.7 ppm, compared to the flat shift correction method (Figure 3). This suggests that most of the errors stem from a constant offset from the true value. However, because multi-point linear regression also showed a meaningful (~20%) reduction in the median RMSE, it is reasonable to conclude that scaling errors are also present in low-cost NDIR sensors.

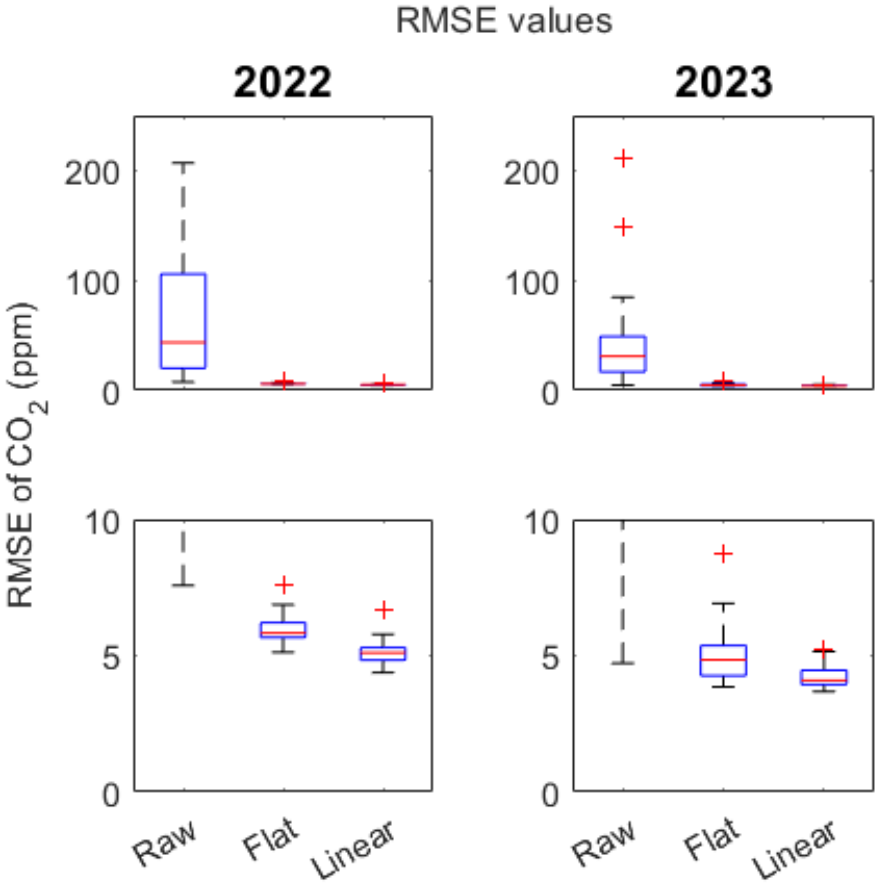

Figure 3. Box diagram of RMSE values from CO_2 measurements made with HT-2000 at Bongcheon Intersection in 2022 and 2023 (against LI-840a). While both methods (flat-shift and multi-point linear regression) reduced errors significantly, multi-point linear regression demonstrated a lower RMSE by about 0.7 ppm. The lower figures are enlarged sections of the top figures.

For the measurement at Guryong Tunnel on 21 November 2024, we compare the two correction methods (two-point correction method by having the HT-2000 kit measure two gases of known CO_2 concentration, vs. multiple-point linear regression). The two-point method resulted in a significant increase in the measured CO_2 concentration and a notable rise in the RMSE values, because the measured CO_2 concentration within the tunnel exceeded the concentrations of the gas canisters used for the two-point regression. In contrast, the multi-point regression method led to a substantial decrease in RMSE (median RMSE 79.6 ppm before correction vs. 12 ppm after correction; Figure 4)

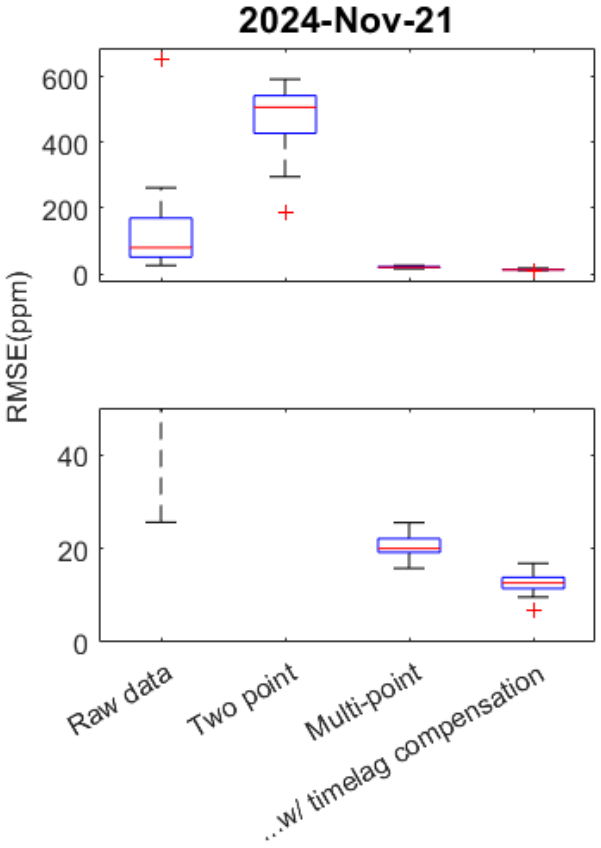

Figure 4: Box diagram of RMSE of CO_2 concentrations measured in Guryong Tunnel with HT-2000 (against LI-840a). The HT-2000 meters were corrected with results from a LI-840a device measuring from the same spot. The lower figure is an enlarged section of the top figure.

2.3.4 Effect of time lag correction

For high temporal resolution measurements, synchronisation between devices is crucial; even minor timing discrepancies can lead to inaccurate representations of CO_2 movement. In this case, the time lag was calculated algorithmically using LI-840a as the ground truth, and the HT-2000 meters' time series were aligned accordingly. The effect of time-lag correction varied between sessions. For the 2022 session, the average time lag of the HT-2000 devices (compared to LI-840a) was 38.58 s, and

failing to apply time-lag correction resulted in a median RMSE increase of approximately 2 ppm. By contrast, for the 2023 session, the average time lag was 19.95 s, and not applying the correction led to a median RMSE increase of less than 0.5 ppm. The time delay of the sensors varied significantly between sessions, which can be explained by several factors. The first is the discrepancy between the internal clocks of the HT-2000 sensors and the laptop used to log HT-2000 data. However, because HT-2000 devices went through a synchronisation step before the measurements, such a large degree of variation does not seem plausible. Instead, we hypothesised that the $MgClO_4$ vapour trap used for the LI-840a kit affects the airflow within the airlines; airflow can vary depending on whether the $MgClO_4$ grains are packed closely or loosely. The optimal smoothing windows for the 2022 and 2023 sessions were different (131 s for 2022, 232 s for 2023), which may also have been affected by the packing status of the $MgClO_4$ grains. Further, since the HT-2000 kits do not have mechanical ventilation system, and since the SenseAir S8 sensors have their air inlet covered by fabric filter, the time delay of each HT-2000 kit could be affected by the direction of the placed kits, or the degree of contamination each S8 sensors have.

2.3.5 Effect of temperature and relative humidity in multi-point linear regression

Absolute humidity and temperature were included as factors in the multi-point linear regression during Bongcheon Intersection measurements, because we suspected residual interference in the low-cost NDIR sensor. To evaluate the impact of humidity and/or temperature in the regression, we performed a multi-point linear regression with different combinations of factors. Including absolute humidity or temperature did not significantly change the median RMSE values, as shown in Figure 5 (ranging from 5.10 to 5.21 ppm in 2022 and from 4.09 to 4.71 ppm in 2023). Thus, it was not included as factors during Guryong Tunnel measurements.

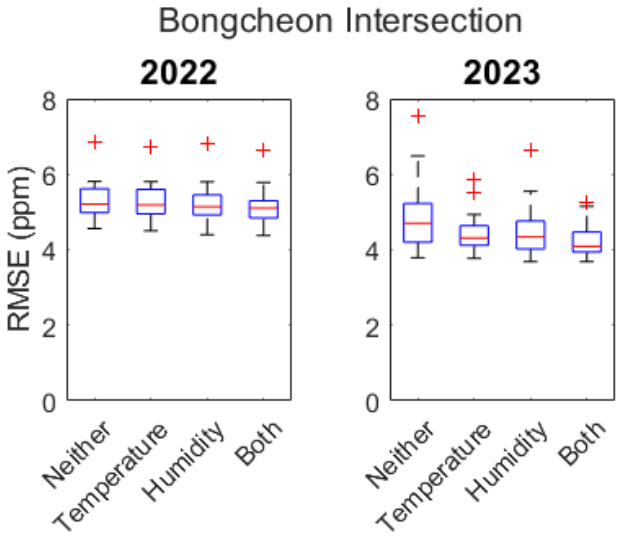

Figure 5: Box diagram of RMSE values from CO_2 measurements made with HT-2000 at Bongcheon Intersection in 2022 and 2023. The x-axis indicates which variables were included in the linear regression.

2.3.6 Evaluation of the feasibility of a common set of regression coefficients

Because the meters (and their internal sensors) are from the same company and model, it might seem reasonable to use a common set of regression coefficients for convenience and scientific consistency. However, the correction constants vary significantly, and using an average set of constants leads to significantly larger error values compared to individually corrected results. This finding aligns with previous studies (Martin et al., 2017), in which averaging the regression coefficients led to a substantial increase in error (Figure 6).

In Martin et al. (2017), the experiment was conducted using Raspberry Pi-based modules, and extra effort was made to synchronize the sensors. The authors reported up to a 20-fold increase in RMSE values when a generalised set of coefficients was used to calibrate the sensors.

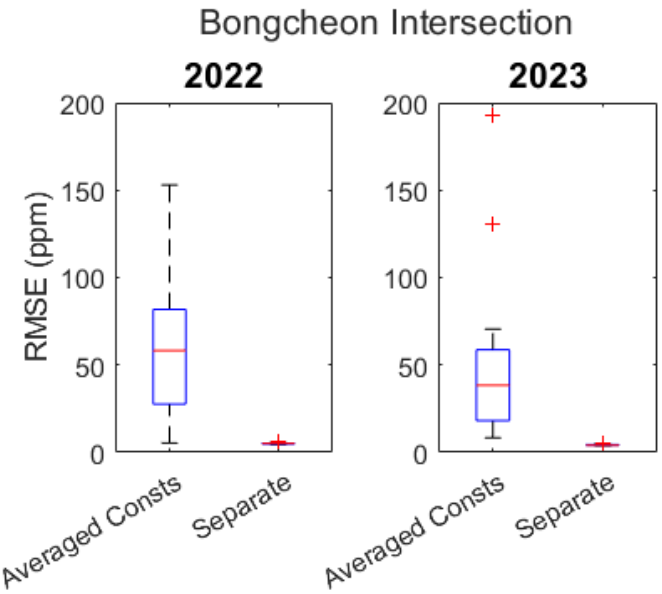

Figure 6: Box diagram of RMSE values from CO_2 measurements made with HT-2000 at Bongcheon Intersection in 2022 and 2023, using separate constants vs. an averaged set of constants. Median values increased significantly when using averaged constants for correction.

3 Results

3.1 Correction at Bongcheon Intersection

For the Bongcheon Intersection measurement, we first measured the CO_2 concentration simultaneously with LI-840 and HT-2000 on the same spot near the centre of the intersection to provide information for correction. Table 1 shows the average bias

and time lag for each HT-2000 meter, along with the root mean square error (RMSE) values before and after correction. As indicated, the bias varied significantly across meters, with the worst-case deviation exceeding 200 ppm compared with the LI-840a measurements. Before linear correction, the median RMSE values were 42.07 ppm in 2022 and 30.60 ppm in 2023. After the correction, the median RMSE values decreased significantly to 5.10 ppm in 2022 and 4.09 ppm in 2023. Additionally, the RMSE for the CO_2 values compared with the LI-840a measurements (taken over the same period) is provided. RMSE was computed using the following equation:

$$RMSE = \sqrt{\frac{\sum_{i=1}^{n}(x_i^p - x_i^k)^2}{n}}$$

where i is the time point; x_i^p is the CO_2 value from the corrected HT-2000 sensor labelled p at ith time point; and x_i^k is the CO_2 value from the LI-840a device at the same time point. The results demonstrate that multi-point linear regression significantly the reduced the RMSE values by approximately one order-of-magnitude, from approximately 50 ppm to 5 ppm (Figure 7c and 7e).

225 **Table 1: Flat bias, time lag, RMSE (compared to LI-840a) for data pre- and post-correction from 2022 and 2023 Bongcheon Intersection measurements.**

2022		Root Mean Square values against LI-840a device			2023		Root Mean Square values against LI-840a device	
Bias from LI-COR (ppm)	Time-lag (s)	Before correction (RMSE, ppm)	After correction (RMSE, ppm)	Sensor labels	Bias from LI-COR (ppm)	Time-lag (s)	Before correction (RMSE, ppm)	After correction (RMSE, ppm)
138.07	39	138.85	5.15	A	-19.64	17	19.73	4.02
227.12	37	227.80	4.85	B				
-2.75	37	8.26	4.57	C	-31.10	27	31.11	3.92
-36.14	43	36.59	5.36	D	-4.83	15	7.13	4.21
				F	-50.71	27	50.61	4.56
				G	25.17	22	26.56	5.15
-43.61	37	43.73	5.13	H	-23.09	7	23.13	4.12
205.55	40	206.26	5.30	I				
172.97	34	173.65	4.38	J	-15.33	16	15.47	3.72
62.60	38	63.71	5.54	K	5.63	21	7.54	3.93
58.29	41	59.43	4.98	M	39.85	13	40.57	3.97
18.30	35	20.35	4.71	N	148.23	14	148.71	3.95
40.79	36	42.07	4.83	O	84.70	23	85.28	4.42
12.35	34	15.05	5.20	P	36.76	16	37.44	3.83
76.77	44	77.80	4.94	Q	2.06	24	4.92	3.69
-11.53	36	13.80	5.10	R	59.79	32	60.90	5.26
-21.68	41	23.18	6.64	S	-17.05	16	17.58	4.49
141.81	37	142.56	4.42	T				
28.67	36	30.39	5.22	U	-30.18	9	30.09	4.18
				V	7.82	19	9.87	4.02
				W	-46.29	26	46.23	4.85
14.42	36	16.86	4.86	X	47.02	25	47.73	4.45
-14.86	43	16.81	5.78	Y				
				Z	210.42	33	210.90	4.06

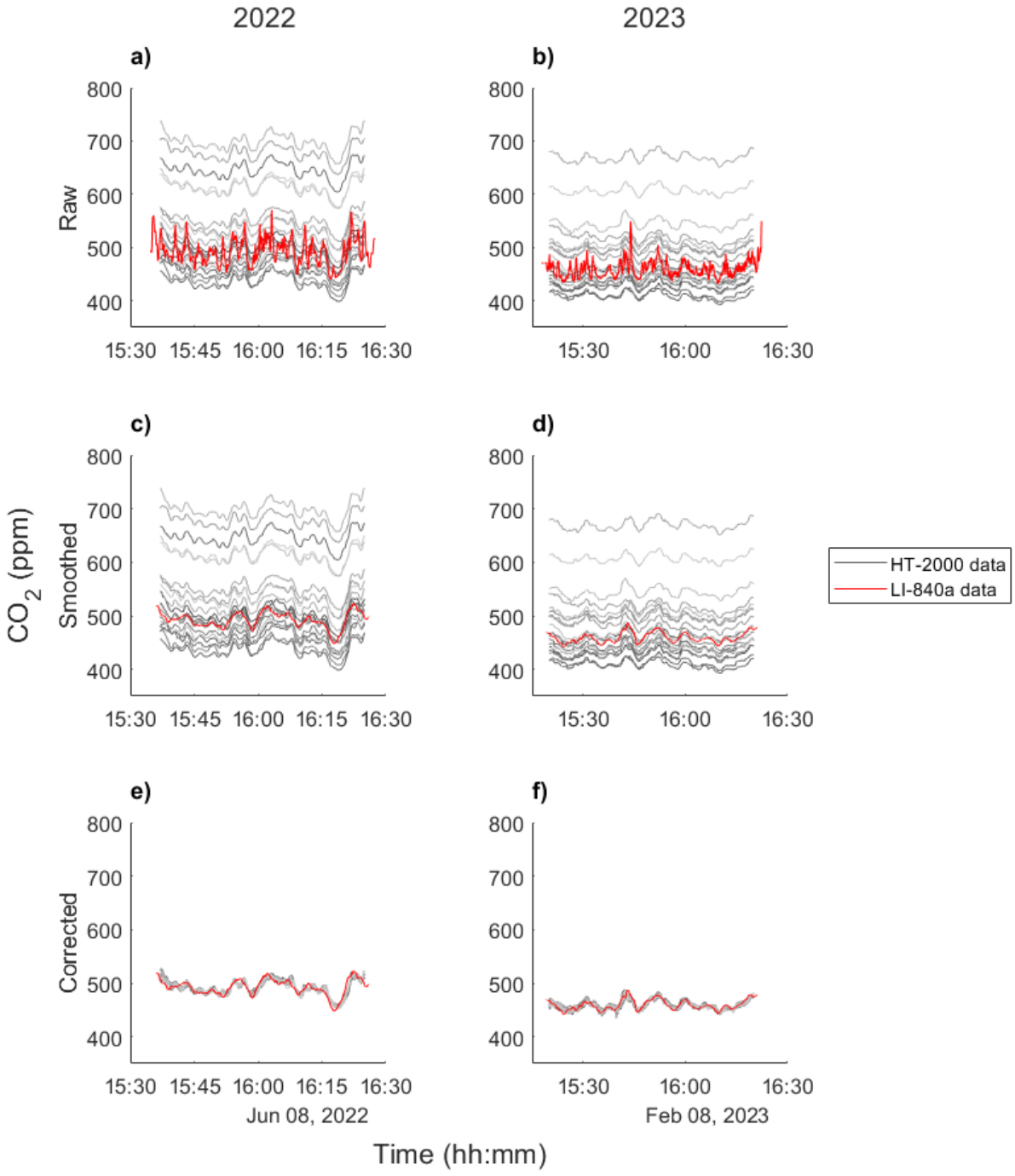

Figure 7. CO_2 concentrations measured in Bongcheon Intersection, before and after correction. a) and b) Plots of CO_2 values measured by HT-2000 (grayscale) and LI-840a (red), before any correction was applied. c) and d) The LI-840a values smoothed with a 137-second window. Note that the HT-2000 sensor values closely follow the smoothed LI-840 values, though with fixed offsets. e) and f) Results after linear correction of the HT-2000 meters.

3.2 CO_2 concentration map at Bongcheon Intersection

The time-averaged, corrected CO_2 values from the meters ranged from 348 to 482 ppm during the 2022 session, and from 457 to 512 ppm during the 2023 session. The corrected CO_2 concentrations obtained from each HT-2000 were then interpolated temporally for each HT-2000 sensor, then interpolated spatially using the *scatteredinterpolant* function in MATLAB which uses Delaunay triangulation then performs linear interpolation on each of the triangles on default settings. The results showed a distinct peak at the traffic intersection, with concentrations gradually decreasing as the distance from the intersection increased. In addition, the standard deviation of the CO_2 concentrations, which represents the variance, also exhibited a peak at the intersection.

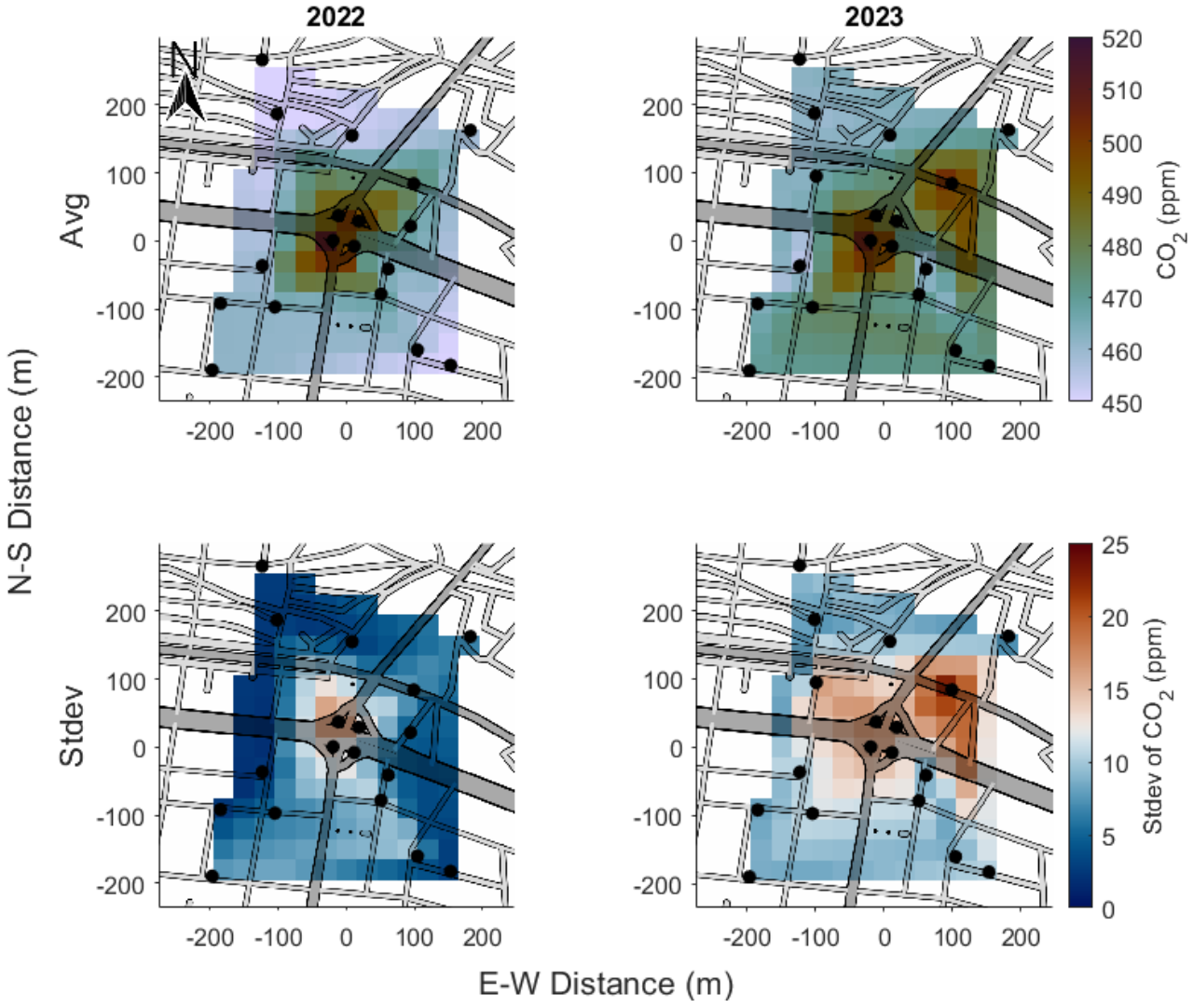

Figure 8. Average and standard deviation of CO_2 concentration over time of Bongcheon Intersection. The top rows show average concentration of CO_2, the bottom rows show standard deviation. The left column shows the result for 2022 session; the right column

shows the result for 2023 session. The standard deviation over time was calculated to show the variation in CO_2 concentration throughout the sessions. © OpenStreetMap Contributors 2024. Distributed under the Open Data Commons Open Database License (ODbL) v1.0.

3.3 CO_2 concentration levels in the Guryong Tunnel

In the Guryong Tunnel, a clear CO_2 gradient was observed, with higher concentrations near the exit. While the entrance showed minimal temporal variation, the variability in CO_2 levels increased toward the exit. Additionally, CO_2 peaks occurred later at positions closer to the exit (Figure 9), consistent with the piston effect induced by traffic movement (Chen et al., 1997). During the November measurements (post-correction), the highest recorded CO_2 concentration was 1,116 ppm, and the lowest was 421 ppm. Notable decreases in CO_2 levels were observed at approximately 12 PM and again at 8 PM (Figure 10).

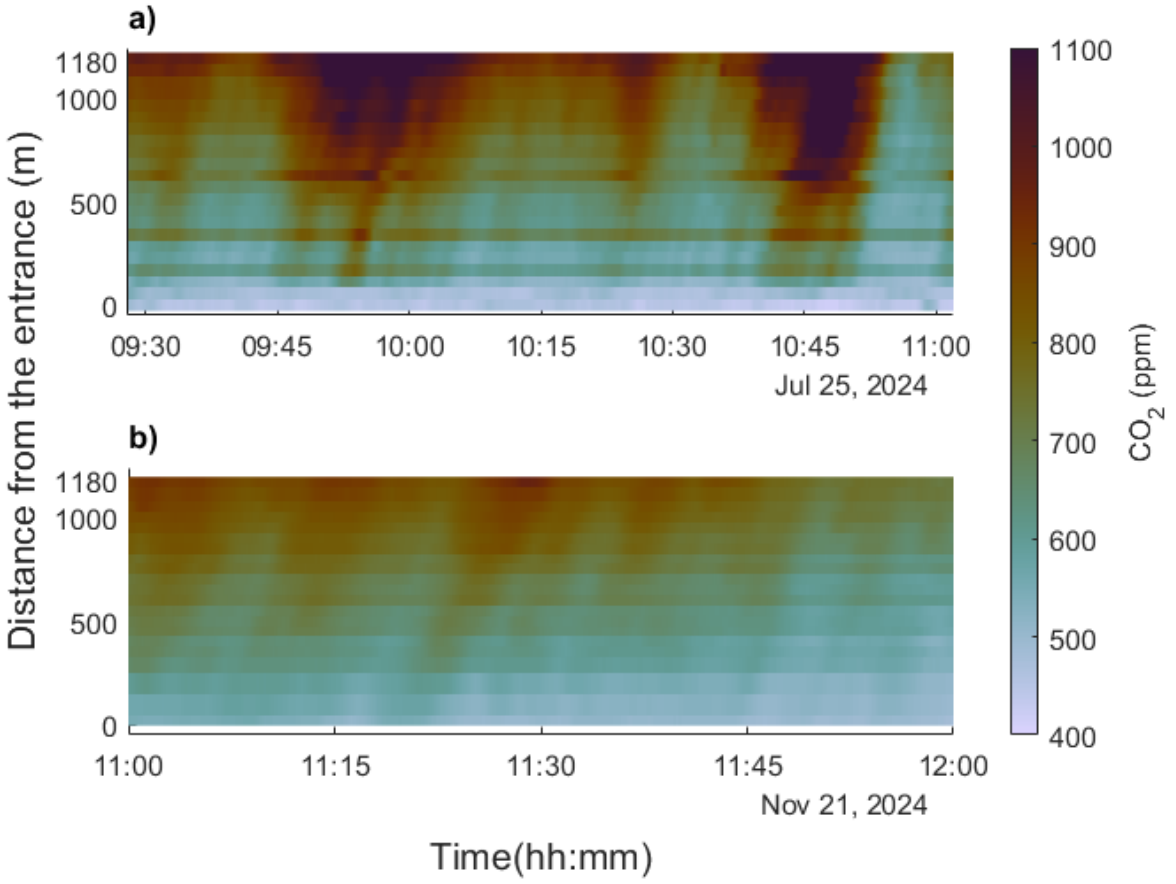

Figure 9. CO_2 values measured (corrected) at the Guryong Tunnel, on July 25 (a) and November 21 (b, segment) in 2024. Data was temporally resampled from 10 s between each data points to 1 s using linear interpolation, then spatially interpolated each second using 1-dimensional linear interpolation. The y-axis is measured from the tunnel entrance, and the 1180m mark represents the exit of the tunnel.

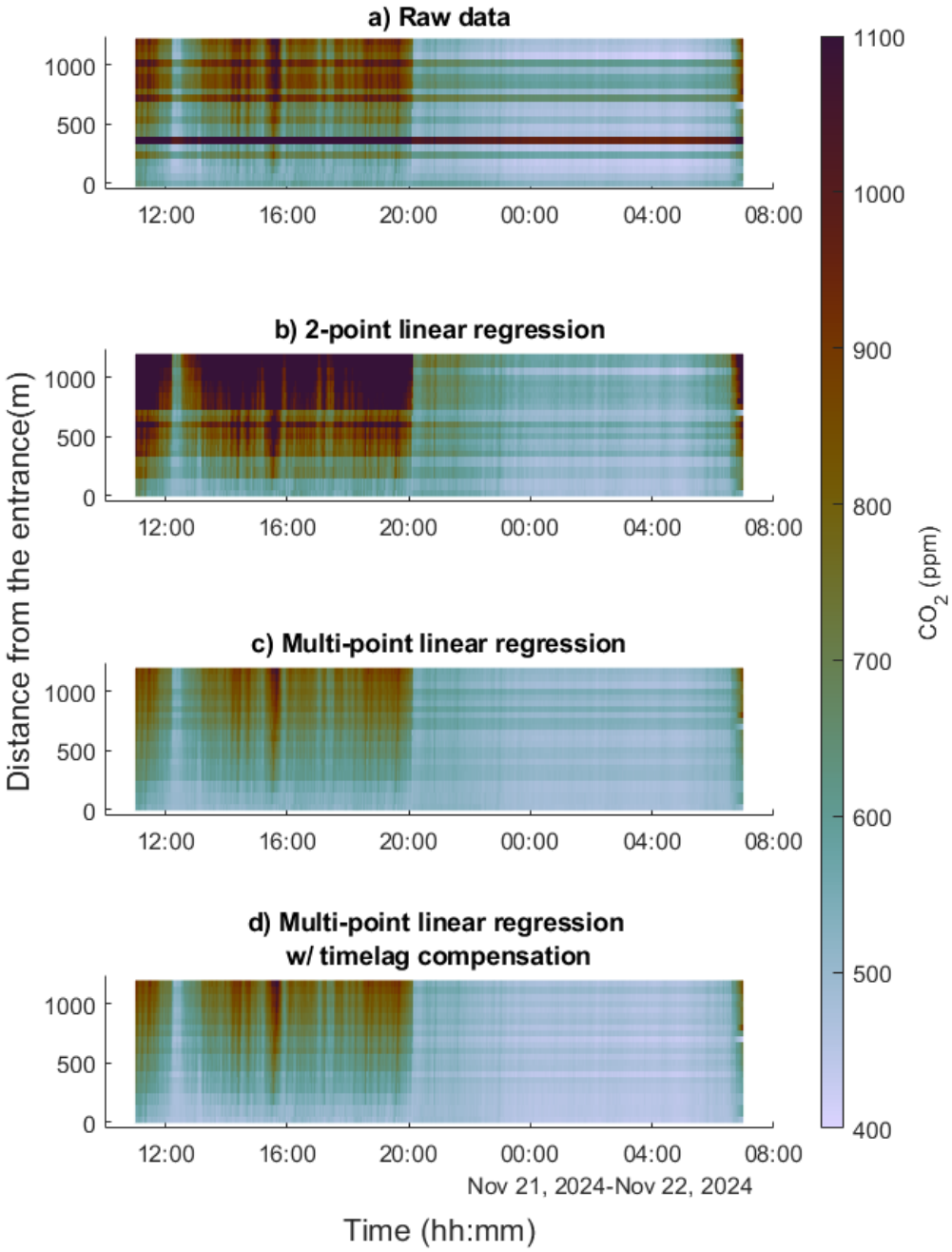

Figure 10: Comparison of CO_2 values measured at Guryong Tunnel, corrected with different methods: raw data (a) vs 2-point regression (b) vs multi-point linear regression (c, d). Correction using linear regression shows significantly lower CO_2 concentration compared to 2-point correction method. Bottom image (d) is from multi-point linear regression attempt with time-lag compensation, compared to (c).

4 Discussion

4.1 Main factors influencing CO_2 distribution at Bongcheon Intersection

As shown in Figure 8, traffic crossings exhibited the greatest variation and highest CO_2 concentrations. To analyse this further, videos were created to track CO_2 concentrations and their trends. In the CO_2 concentration videos (supplementary materials S1 and S3), small fluctuations were observed at the junction. Videos showing the rate of CO_2 concentration change (supplementary materials S2 and S4) revealed quasi-periodic variations at the junction. The four sensors positioned at the junction were located on traffic islands, where the primary source of CO_2 is vehicular traffic. Specifically, vehicles idling at a red light contribute to a concentration build-up at fixed locations, whereas vehicles in the right-turn lane do not have the same effect. Therefore, it is reasonable to associate these CO_2 changes with traffic signal cycles. A similar build-up was also observed in the northeastern corner of the 2023 video (supplementary material S4), where the responsible sensor was positioned near a traffic crossing. Additionally, we noted a local increase in CO_2 levels outside the intersection, likely caused by smaller, local traffic loads.

Our methods do not incorporate any information about the urban landscape, such as building locations or shapes, nor do they rely on air-transport data. They can also be integrated with atmospheric modeling by replacing the spatial interpolation step with a suitable modeling approach. Because the sensors are low-cost, their numbers can be increased substantially, enabling much more comprehensive monitoring.

4.2 Main factors influencing CO_2 distribution in the Guryong Tunnel

The meters at the tunnel entrance showed slight temporal variation compared to those at the exit. Additionally, a noticeable trend emerged: both the CO_2 concentration and its variability increased as traffic moved through the tunnel. This observation aligns with the previously described piston effect caused by traffic flow (Chen et al., 1997). Data from the 21 November measurements at the Guryong Tunnel revealed a sharp drop in CO_2 concentration after 8 PM. It was hypothesised that the CO_2 concentration approximately corresponds to the number of vehicles in the tunnel at a given time (vehicle density). To estimate this, the following equation was devised:

$$N = \frac{(Number\ of\ entering\ cars\ per\ unit\ time)}{(Traffic\ velocity)} \times (Tunnel\ length)$$

where N is the vehicle density in the tunnel at a specific time. Although the number of vehicles entering the tunnel remained fairly constant around 8 PM, the average traffic velocity increased significantly, leading to a reduction in vehicle density. This

explains the rapid decrease in CO_2 concentration observed (Figure 11). 4.3 Limitations of this experiment

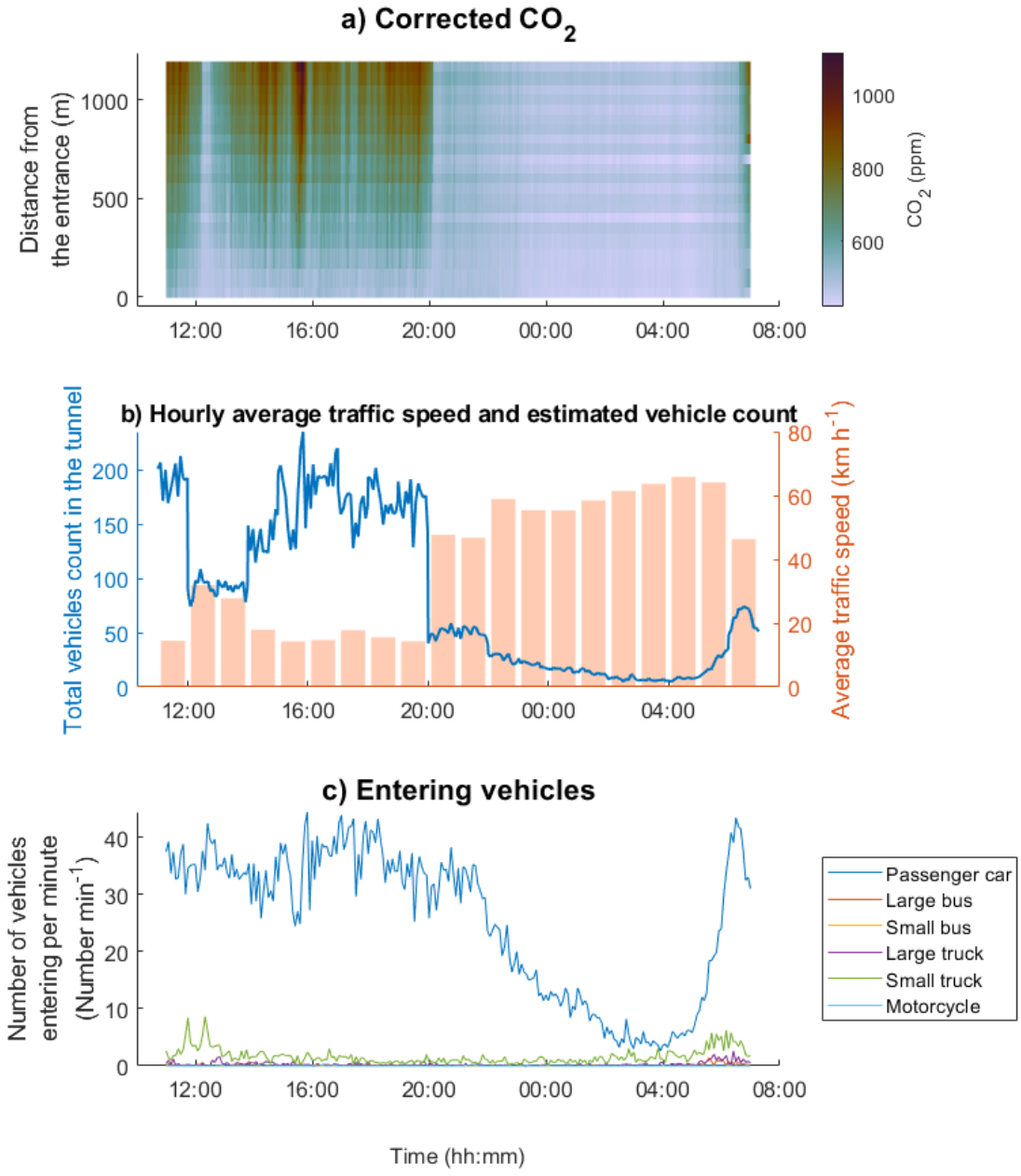

290

Figure 11. CO_2 concentration in the Guryong Tunnel, calculated number of vehicles inside the tunnel, and number of entering vehicles over time. (a) is identical to (d) in Figure 5; it represents the result of multi-point linear regression with time-lag correction. Total vehicle count (b) was calculated from interpolated number of vehicles entering the tunnel (from Seoul Facilities Corporation, private communication) and hourly averaged traffic velocity for Eonju-ro (Seoul Transport Operation and Information Service;
295 **https://topis.seoul.go.kr/refRoom/openRefRoom_1.do). No significant drop in entering traffic (c) is observed around 8 PM, but**

average traffic speed increases significantly around at that time. The increased speed decreases the time a vehicle spends in the tunnel ultimately reducing the total number of vehicles inside.

5 Conclusions

This study demonstrates the feasibility of using low-cost NDIR sensors, such as the HT-2000, for high-resolution urban CO_2 monitoring when combined with effective correction techniques. By employing multi-point linear regression and time-lag correction, we significantly reduced the median RMSE of the HT-2000 sensors from over 10% to just 1–2% of the measured values, achieving an order-of-magnitude improvement in accuracy. This approach enables the deployment of large-scale sensor networks for detailed spatial and temporal monitoring of CO_2 concentrations in urban environments, where emissions exhibit significant variability owing to diverse land-use patterns and dynamic traffic conditions. The results highlight the importance of individual sensor corrections, because the use of a common set of regression coefficients introduces substantial errors. Furthermore, this study underscores the influence of traffic dynamics on localised CO_2 distributions, as evidenced by the quasi-periodic variations at the Bongcheon Intersection and the piston effect observed in the Guryong Tunnel. These findings provide valuable insights for urban CO_2 flux estimation and underscore the potential of low-cost sensors to support targeted emission-reduction strategies. Future studies should focus on optimising correction methods and expanding sensor networks to capture broader urban emission patterns, ultimately contributing to more accurate and actionable climate mitigation efforts.

Author Contribution. Jinho Ahn designed the experiments, JaeYoung Park and Jeongeun Kim carried them out. JaeYoung Park and Nasrin Salehnia developed code to analyze the results. JaeYoung Park prepared the manuscript with contributions from all co-authors.

Acknowledgements. We would like to thank KwangJin Yim at the Center for Cryospheric Sciences, Seoul National University, for his dedicated assistance and support with air sample collection. We also thank Gangnam Roadway Management for the permission to enter the tunnel, and for the supplied traffic data. Maps were obtained from Openstreetmap (openstreetmap.org/copyright). The images were made with MATLAB Version: 23.2.0.2391609 (R2023b) Update 2. The color schemes are from MATLAB and Crameri et al. (2020). This study is supported by National Research Foundation of Korea (2018R1A5A1024958; 2020H1D3A1A04081353; RS-2023-00291696; RS-2023-00278926) grant to JA.

References

Arzoumanian, E., Vogel, F. R., Bastos, A., Gaynullin, B., Laurent, O., Ramonet, M., and Ciais, P.: Characterization of a commercial lower-cost medium-precision non-dispersive infrared sensor for atmospheric CO_2 monitoring in urban areas, Atmos. Meas. Tech., 12, 2665–2677, https://doi.org/10.5194/amt-12-2665-2019, 2019.

Band, L.E., Cadenasso, M.L., Grimmond, C.S., Grove, J.M., Pickett, S.T.A.: Heterogeneity in Urban Ecosystems: Patterns and Process. In: Lovett, G.M., Turner, M.G., Jones, C.G., Weathers, K.C. (eds) Ecosystem Function in Heterogeneous Landscapes. Springer, New York, NY. https://doi.org/10.1007/0-387-24091-8_13, 2005

Burba, G., Madsen, R., Feese, K.: Eddy Covariance Method for CO2 Emission Measurements in CCUS Applications: Principles, Instrumentation and Software, Energy Procedia, 40, 329-336, https://doi.org/10.1016/j.egypro.2013.08.038, 2013

Chen, T.Y., Lee, Y.T., and Hsu, C.C.: Investigations of piston-effect and jet fan-effect in model vehicle tunnels, J. Wind Eng. Ind. Aerod. 73, 99-110, https://doi.org/10.1016/S0167-6105(97)00281-X, 1998.

Cuadros-Rodríguez, L., Gámiz-Gracia, L., Almansa-López, E., Bosque-Sendra, J.: Calibration in chemical measurement processes. II. A methodological approach, TrAC-Trend. Anal. Chem., 20, 620-636, https://doi.org/10.1016/S0165-9936(01)00111-X, 2001

Gately, C. and Hutyra, L. R.: Large uncertainties in Urban-Scale carbon emissions. J. Geophys. Res-Atmos, 122, 11242-11260, https://doi.org/10.1002/2017jd027359, 2017.

Gurney, K. R., Liang, J., OKeeffe, D., Patarasuk, R., Hutchins, M., Huang, J., Rao, P. and Song, Y.: Comparison of global downscaled versus Bottom-Up fossil fuel CO_2 emissions at the urban scale in four U.S. urban areas, J. Geophys. Res-Atmos, 124, 2823–2840, https://doi.org/10.1029/2018jd028859, 2019.

Gurney, K. R., Liang, J., Patarasuk, R., Song, Y., Huang, J., and Roest, G.: The Vulcan Version 3.0 High-Resolution Fossil Fuel CO_2 Emissions for the United States, J. Geophys. Res-Atmos, 125, e2020JD032974, https://doi.org/10.1029/2020jd032974, 2020.

Han, P., Mei, H., Liu, D., Zeng, N., Tang, X., Wang, Y., and Pan, Y.: Calibrations of low-cost air pollution monitoring sensors for CO, NO_2, O_3, and SO_2, Sensors-Basel, 21, 1–18, https://doi.org/10.3390/s21010256, 2021.

Hong. S., Kim. J., Byun. Y., Hong. J., Hong. J., Lee. K., Park. Y., Lee. S., and Kim. Y.: Intra-urban Variations of the CO_2 Fluxes at the Surface-Atmosphere Interface in the Seoul Metropolitan Area, Asia-Pac. J. Atmos. Sci., 59, 417-431, https://doi.org/10.1007/s13143-023-00324-6, 2023.

HTi: HT-2000 CO_2 meter, https://hti-instrument.com/products/ht-2000-co2-meter, retrieved 2023.

Imasu, R. and Tanabe, Y.: Diurnal and Seasonal Variations of Carbon Dioxide (CO_2) Concentration in Urban, Suburban, and Rural Areas around Tokyo, Atmosphere-Basel, 9, 367, https://doi.org/10.3390/atmos9100367, 2018.

Intergovernmental Panel on Climate Change (IPCC): Changing State of the Climate System. In Climate Change 2021: The Physical Science Basis, 287–422, Cambridge University Press. https://doi.org/10.1017/9781009157896.004, 2021.

Kiel, M., Eldering, A., Roten, D., Lin, J. C., Feng, S., Lei, R., Lauvaux, T., Oda, T., Roehl, C. M., Blavier, J. L. and Iraci, L. T. Urban-focused satellite CO_2 observations from the Orbiting Carbon Observatory-3: A first look at the Los Angeles megacity, Remote Sens. Environ., 258, 112314, https://doi.org/10.1016/j.rse.2021.112314, 2021.

Korea Electric Power Corporation: Statistics of Electric Power in Korea (136-139), https://home.kepco.co.kr/kepco/KO/ntcob/list.do?boardCd=BRD_000099&menuCd=FN05030103, retrieved 2023.

Kort, E. A., Frankenberg, C., Miller, C. E., and Oda, T.: Space-based observations of megacity carbon dioxide. Geophys. Res. Lett., 39, L17806, https://doi.org/10.1029/2012gl052738, 2012.

Martin, C. R., Zeng, N., Karion, A., Dickerson, R. R., Ren, X., Turpie, B. N. and Weber, K. J.: Evaluation and environmental correction of ambient CO_2 measurements from a low-cost NDIR sensor, Atmos. Meas. Tech., 10, 2383–2395, https://doi.org/10.5194/amt-10-2383-2017, 2017.

Korean Ministry of Culture, Sports and Tourism: "South Korea – Summary". https://www.korea.net/AboutKorea/Society/South-Korea-Summary, retrieved 17 July 2024.

Müller, M., Graf, P., Meyer, J., Pentina, A., Brunner, D., Pérez-Cruz, F., Hüglin, C. and Emmenegger, L.: Integration and calibration of non-dispersive infrared (NDIR) CO_2 low-cost sensors and their operation in a sensor network covering Switzerland. Atmos. Meas. Tech, 13, 3815–3834, https://doi.org/10.5194/amt-13-3815-2020, 2020.

Olivo, Y., Hamidi, A., Ramamurthy, P.: Spatiotemporal variability in building energy use in New York City. Energy, 141, 1393-1401, https://doi.org/10.1016/j.energy.2017.11.066, 2017.

Park, C., Jeong, S., Park, M. S., Park, H., Yun, J., Lee, S. S., and Park, S. H.: Spatiotemporal variations in urban CO_2 flux with land-use types in Seoul., Carbon Balance Manage, 17, 3, https://doi.org/10.1186/s13021-022-00206-w, 2022

Roche, S., Strong, K., Wunch, D., Mendonca, J., Sweeney, C., Baier, B. C., Biraud, S., Laughner, J. L., Toon, G. C. and Connor, B. J.: Retrieval of atmospheric CO_2 vertical profiles from ground-based near-infrared spectra, Atmos. Meas. Tech, 14(4), 3087–3118, https://doi.org/10.5194/amt-14-3087-2021, 2021.

Rosenzweig, C., Solecki, W., Hammer, S. A., and Mehrotra, S.: Cities lead the way in climate–change action. Nature, 467(7318), 909–911, https://doi.org/10.1038/467909a, 2010.

Seoul Carbon Neutrality Support Center, 2022 Greenhouse Gas Inventory for Seoul. https://seoulnetzero.si.re.kr/archives/data/, accessed 2025.

Seoul Metropolitan Government: Information on the number of passengers boarding and disembarking each subway line and station in Seoul. http://data.seoul.go.kr/dataList/OA-12914/S/1/datasetView.do, accessed 2023.

Spinelle, L., Gerboles, M., Villani, M., Aleixandre, M. and Bonavitacola, F.: Field calibration of a cluster of low-cost commercially available sensors for air quality monitoring. Part. B: NO, CO and CO_2. Sensor Actuat. B-Chem. 238, 706-715, https://doi.org/10.1016/j.snb.2016.07.036, 2017.

United Nations, Department of Economic and Social Affairs, Population Division.: World Urbanization Prospects: The 2018 Revision, Online Edition. https://population.un.org/wup/Download/, 2018.

Vardag, S. N., Maiwald, R.: Optimising urban measurement networks for CO2 flux estimation: a high-resolution observing system simulation experiment using GRAMM/GRAL, Geosci. Model Dev., 17, 1885–1902, https://doi.org/10.5194/gmd-17-1885-2024, 2024

SenseAir: SenseAir S8 Residential Product Specification. https://rmtplusstoragesenseair.blob.core.windows.net/docs/publicerat/PSP107.pdf, accessed 12 Feb 2025.